#### Society for Mathematical Biology

#### ORIGINAL ARTICLE



# Modeling Antiretrovial Treatment to Mitigate HIV in the Brain: Impact of the Blood-Brain Barrier

Colin T. Barker<sup>1</sup> · Feng-Bin Wang<sup>2,3,4</sup> · Naveen K. Vaidya<sup>5,6,7</sup>

Received: 18 December 2022 / Accepted: 4 August 2023 / Published online: 21 September 2023 © The Author(s), under exclusive licence to Society for Mathematical Biology 2023

#### **Abstract**

Current research in Human Immunodeficiency Virus (HIV) focuses on eradicating virus reservoirs that prevent or dampen the effectiveness of antiretroviral treatment (ART). One such reservoir, the brain, reduces treatment efficacy via the blood-brain barrier (BBB), causing an obstacle to drug penetration into the brain. In this study, we develop a mathematical model to examine the impact of the BBB on ART effectiveness for mitigating brain HIV. A thorough analysis of the model allowed us to fully characterize the global threshold dynamics with the viral clearance and persistence in the brain for the basic reproduction number less than unity and greater than unity, respectively. Our model showed that the BBB has a significant role in inhibiting the effect of ART within the brain despite the effective viral load suppression in the plasma. The level of impact, however, depends on factors such as the CNS Penetration Effectiveness (CPE) score, the slope of the drug dose-response curves, the ART initiation timing, and the number of drugs in the ART protocol. These results suggest that reducing the plasma viral load to undetectable levels due to some drug regimen may not necessarily indicate undetectable levels of HIV in the brain. Thus, the effect of the BBB on viral suppression in the brain must be considered for developing proper treatment protocols against HIV infection.

Viral Information Institute, San Diego State University, California, San Diego, USA



Naveen K. Vaidya nvaidya@sdsu.edu

Department of Mathematics and Computer Science, Drury University, Missouri, USA

Department of Natural Science in the Center for General Education, Chang Gung University, Taoyuan 333, Guishan, Taiwan

Community Medicine Research Center, Chang Gung Memorial Hospital, Keelung 204, Keelung Branch, Taiwan

National Center for Theoretical Sciences, National Taiwan University, Taipei 106, Taiwan

Department of Mathematics and Statistics, San Diego State University, California, San Diego, USA

<sup>6</sup> Computational Science Research Center, San Diego State University, California, San Diego, USA

**Keywords** HIV in the brain · Antiretroviral therapy

## 1 Introduction

Human Immunodeficiency Virus (HIV) represents one of the most serious global health issues, with approximately 36.7 million people currently living with HIV, a number that grows by roughly 1.5 million per year (United Nations Programme 2019). Despite impressive strides in antiretroviral therapy (ART), there is no known cure for HIV. Several obstacles are yet to be overcome in this ongoing search for an HIV cure. For instance, the establishment of physiological virus reservoirs, such as the brain, gut, liver, and reproductive organs (Abreu et al. 2019; Fois and Brew 2015; Gray et al. 2014; Hellmuth et al. 2015; Nath 2015), and infected cells not immediately proliferating free virions, whether they are long-lived or latently infected, all contribute significant hurdles to a cure for HIV.

The brain, in particular, may act as the viral reservoir, and viral replication within it may contribute to viral rebound within the plasma (Ash et al. 2021; Bates and Watts 1988; Beguelin et al. 2016; Kincer et al. 2023; Osborne et al. 2020) upon cessation of treatment. In addition, HIV establishment in the brain has been shown to lead to HIV-associated neurocognitive disorders (HAND), such as dementia and early-onset encephalitis (Pauza 1988). Thus, while each reservoir type deserves considerable attention, there is an urgency to develop ART protocols to mitigate HIV in the brain.

HIV can enter the brain by crossing the Blood-Brain Barrier (BBB) via infected macrophages, even during early infection (Clements et al. 2022; Fois and Brew 2015; Koppensteiner et al. 2012; Pauza 1988; Strazielle et al. 2016). Notably, the BBB affects the permeability of drugs into the brain, as measured by Letendre (2011) in terms of a CNS Penetration Effectiveness (CPE) score. We note that the other viral reservoirs may also express suboptimal drug penetration (Kepler and Perelson 1998). However, there is a lack of a numerical penetration measure, and we did not consider other reservoirs in this study. The smaller proportion of drugs in the brain may allow ongoing viral replication despite undetectable viral loads in the plasma. Moreover, the efficacy of an ART drug depends on its pharmacodynamics, and some drugs have an efficacy as low as 68% (Louie et al. 2003). Furthermore, these pharmacodynamics play a significant role in the evolution of HIV (Rosenbloom 2012). Therefore, the CPE score, as well as the efficacy of HIV drugs, must be taken into account to develop proper treatment protocols for HIV control in the brain.

Mathematical models have offered insights into the viral dynamics in the brain (Huang et al. 2017; Roda et al. 2017) and the latent reservoirs (Callaway and Perelson 2002; Stafford et al. 2000; Vaidya et al. 2010; Vaidya and Rong 2017). However, limited research exists on the effect of ART on mitigating HIV in the brain and the role of BBB on treatment effectiveness. In this study, we develop a mathematical model to analyze the role of BBB on the overall treatment effectiveness for HIV in the brain. We consider various potential ARTs by altering key drug parameters, such as the CPE score, the slope of the dose-response curve, and the treatment initiation time. We also thoroughly analyze the model to establish the local and global properties of the HIV infection dynamics in the brain. Our study identifies thresholds for the stability of



infection dynamics and highlights the critical role of the BBB on the optimal outcome of the treatment protocols.

#### 2 Model

## 2.1 Model Development

In our model, we consider six mutually exclusive cell compartments: uninfected CD4+ T cells in the plasma (T), uninfected macrophages in the plasma (M), uninfected macrophages in the brain  $(M_B)$ , often called microglia, infected CD4+ T cells in the plasma  $(T^*)$ , infected macrophages in the plasma  $(M^*)$ , and infected macrophages in the brain  $(M_B^*)$ . In addition, we consider two viral compartments, V and  $V_B$ , representing the concentration of free virions in the plasma and the brain, respectively. We describe the viral dynamics using the following differential equations, and a schematic diagram of the model is presented in Fig. 1.

$$\begin{split} \frac{\mathrm{d}T}{\mathrm{d}t} &= \lambda - \prod_{i=1}^{n} (1 - \varepsilon_i)\beta V T - dT, \\ \frac{\mathrm{d}T^*}{\mathrm{d}t} &= \prod_{i=1}^{n} (1 - \varepsilon_i)\beta V T - \delta T^*, \\ \frac{\mathrm{d}M}{\mathrm{d}t} &= \lambda_M - \prod_{i=1}^{n} (1 - \varepsilon_i)\beta_M V M - \varphi M + \psi M_B - d_M M, \\ \frac{\mathrm{d}M^*}{\mathrm{d}t} &= \prod_{i=1}^{n} (1 - \varepsilon_i)\beta_M V M + \psi M_B^* - \varphi M^* - \delta_M M^*, \\ \frac{\mathrm{d}MB}{\mathrm{d}t} &= \varphi M - \psi M_B - \prod_{i=1}^{n} (1 - \varepsilon_{\pi i})\beta_M V_B M_B - d_M M_B, \\ \frac{\mathrm{d}MB}{\mathrm{d}t} &= \prod_{i=1}^{n} (1 - \varepsilon_{\pi i})\beta_M V_B M_B - \psi M_B^* + \varphi M^* - \delta_M M_B^*, \\ \frac{\mathrm{d}V}{\mathrm{d}t} &= \prod_{i=1}^{n} (1 - \varepsilon_{PIi}) p T^* + \prod_{i=1}^{n} (1 - \varepsilon_{PIi}) p_M M^* - cV, \\ \frac{\mathrm{d}V_B}{\mathrm{d}t} &= \prod_{i=1}^{n} (1 - \varepsilon_{\pi PIi}) p_M M_B^* - cV_B. \end{split}$$

Basic Viral Dynamics in the brain and in the plasma. Uninfected T cells die at a constant rate d and are generated at a rate  $\lambda$ . Uninfected T cells (T) are infected  $(T^*)$  by free virions, V, within the circulation at a rate  $\beta$ . The infected cells then die at a rate  $\delta$ . Infected cells produce viruses and release them into circulation at a rate p per infected cell per day (Vaidya et al. 2016). Similarly, HIV-1 infects uninfected macrophages (M) (Clements et al. 2022; Koppensteiner et al. 2012) at a rate  $\beta_M$ . The infected macrophages  $(M^*)$  produce free virions at a rate p per infected cell per day and die at a rate of  $\delta_M$ . Uninfected macrophages die at a rate of d and are generated at a rate  $\lambda_M$ . In order for a virion to enter the cerebrospinal fluid (CSF)



**105** Page 4 of 29 C. T. Barker et al.

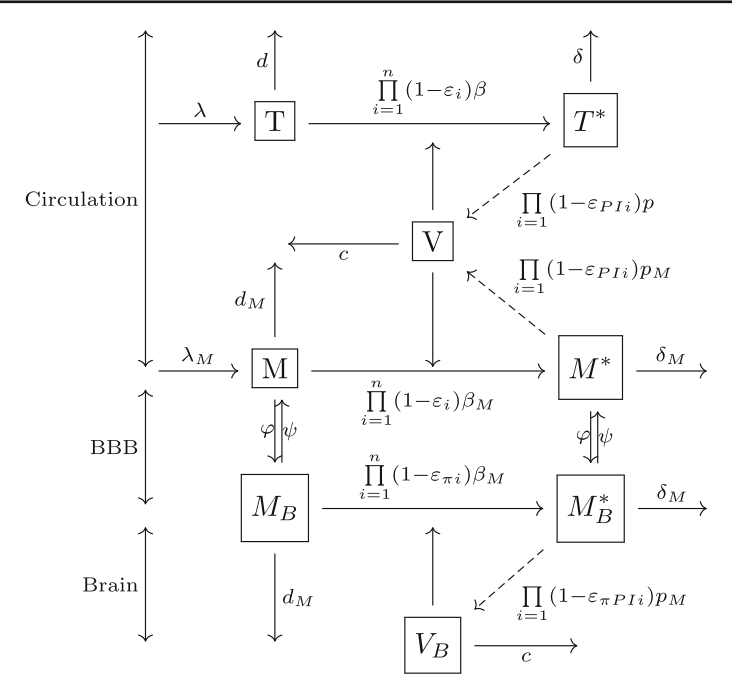


Fig. 1 Schematics of the model for HIV dynamics in the brain under antiretroviral treatment

in the brain, it must pass through the BBB. It is not fully understood what factors modulate the transit of HIV-1 RNA through the BBB into the CNS (Hellmuth et al. 2015); however, research suggests that the virus permeates the integrity of the BBB via an infected macrophage (Koppensteiner et al. 2012). We represent the per capita rate of macrophage transit through the BBB by  $\varphi$ . Macrophages are not known to generate independently within the brain (Prinz and Priller 2014). The uninfected brain macrophages are infected (Bednar et al. 2015; Nath 2015; Prinz and Priller 2014; Schnell et al. 2011) at the constant rate  $\beta_M$ , and infected macrophages produce free virions within the brain at the constant rate  $p_M$ . The free virions V and  $V_B$  die at the per capita clearance rate c. Macrophages exit the brain through the BBB into the bloodstream at a constant rate  $\psi$ . All the basic parameter values are given in Table 1.

**Antiretroviral treatment.** Currently, there are five classes of available ART drugs: Fusion Inhibitors (FIs), Nucleoside reverse transcriptase inhibitors (NRTIs), Nonnucleoside reverse transcriptase inhibitors (NNRTIs), Integrase inhibitors (IIs), and Protease inhibitors (PIs) (CDC 2019). The efficacy of each drug,  $\varepsilon$ , can be calculated by the formula (Vaidya and Rong 2017):

$$\varepsilon = 1 - \left(\frac{1}{1 + \left(\frac{D}{ED_{50}}\right)^m}\right),\,$$



Table 1 Basic model parameters. All the parameter values correspond to the per ml unit

Name	Symbol	Value	Source
Initial Values			
Initial uninfected T-cells	$T_0$	38700	Vaidya et al. (2010)
Initial infected T-cells	$T_0^*$	0	Kumar et al. (2004)
Initial uninfected plasma Macrophages	$M_0$	1463000	Haney (1981)
Initial infected plasma Macrophages	$M_0^*$	0	Kumar et al. (2004)
Initial uninfected CSF Macrophages	$M_{B0}$	20000	Haney (1981)
Initial infected CSF Macrophages	$M_{B0}$	0	Kumar et al. (2004)
Initial plasma free Virions	$V_0$	200 vRNA	Kumar et al. (2004)
Initial CSF free Virions	$V_{B0}$	0	Kumar et al. (2004)
Parameter Values			
Death rate for uninfected T-cells	p	$0.01  (day^{-1})$	Stafford et al. (2000)
Death rate for uninfected Macrophages	$d_M$	$0.00185  (day^{-1})$	Prinz and Priller (2014)
Recruitment rate for T-cells	٧	$387  (day^{-1})$	Calculated
Recruitment rate for Macrophages	$\gamma_M$	$2743.55  (day^{-1})$	Calculated
Viral production from infected T-cells	d	$50000 \text{ (vRNA day}^{-1} \text{ cell}^{-1})$	Chen (2007)
Viral production from infected macrophages	PM	$1000  (\mathrm{vRNA}  \mathrm{day}^{-1} \mathrm{cell}^{-1})$	Schwartz et al. (2018)
Viral clearance rate	2	$23 (day^{-1})$	Ramratnam et al. (1999)
T-cell infection rate	β	$3.5830E-8 (vRNA^{-1} day^{-1})$	Barker and Vaidya (2020)
Death rate for infected T-cells	8	$1.4551  (day^{-1})$	Barker and Vaidya (2020)
Macrophage infection rate	$\beta_M$	$8.653E-10 (vRNA^{-1} day^{-1})$	Barker and Vaidya (2020)
Death rate for infected macrophages	$\delta_M$	$0.2060  (day^{-1})$	Barker and Vaidya (2020)
Rate of macrophage entry into the brain	9	$0.03876  (day^{-1})$	Barker and Vaidya (2020)
Rate of macrophage exit from the brain	Ą	$8.9953 (day^{-1})$	Barker and Vaidya (2020)



**105** Page 6 of 29 C. T. Barker et al.

where m is Hill's coefficient, D is the amount of drug concentration present, and  $ED_{50}$  represents the concentration of drugs required to obtain 50% of the maximal effect. Note that Hill's coefficient provides the slope of the dose-response curve of a given drug. The PIs reduce the viral production rates p and  $p_M$  to  $(1 - \varepsilon_{PIi})p$  and  $(1 - \varepsilon_{PIi})p_M$ , respectively, and drugs from other classes reduce the infection rates p and  $p_M$  to  $p_M$  to  $p_M$  and  $p_M$  to  $p_M$  to  $p_M$  and  $p_M$  to  $p_M$  respectively. Note that integrase inhibitors (IIs) prevent viral-bearing cells from becoming productively infected due to inhibiting viral DNA integration into host DNA. This process has been modeled using a parameter governing integration by von Kleist et al. (2010). Since we have not included a detailed integration process with pre and post proviral integration, we did not require such a separate parameter in our model.

When multiple drugs are used in treatment, we assume no drug-drug interactions, a so-called 'bliss independence' approach, and the residual infection or production can be modeled by the product of residuals of drugs in combination protocol. Therefore, for FIs, IIs, and RTIs, the infection rates are reduced to  $\prod_{i=1}^n (1-\varepsilon_i)\beta$  and  $\prod_{i=1}^n (1-\varepsilon_i)\beta_M$ , and for PIs the viral production rates are reduced to  $\prod_{i=1}^n (1-\varepsilon_{PIi})p$  and  $\prod_{i=1}^n (1-\varepsilon_{PIi})p_M$ , where n represents the number of drugs used in the treatment protocol.

Role of blood brain barrier. The BBB reduces the effectiveness of ART drugs by limiting the amount of concentration in the CSF. A study by Letendre (2011) examined the viral loads in the CSF in the presence of ART drugs and developed a standard measure (CNS penetration effectiveness score, or CPE-score) for the effectiveness of an ART drug in entering the brain. This study utilizes several techniques to gain a qualitative measurement. We note that there are some drug-binding proteins in the blood plasma limiting the total drug effect (Boffito 2003), which are not present in the CSF. Letendre et al. have not included this potential effect (Letendre 2011). However, the study by Letendre (2011) offers a comparative measure of several drugs' effectiveness within the CSF, which we take as a proxy.

Based on the CPE score provided by Letendre (2011), we construct the parameter  $\pi$  to represent the reduced fraction of drugs that enter the brain as follows.

$$\pi = \frac{\text{CPE Score}}{5},$$

where the CPE score (or CNS penetration effectiveness score) ranges from one to four. In the study by Letendre (2011), drugs with a CPE score of one represent minimal CNS penetration, and a CPE score of four represents maximal CNS penetration. However, the perfect penetration is less likely due to the nature of BBB, so we take 5 to scale perfect penetration for the computation purpose. Specifically, for drugs crossing the BBB, we have the following efficacy of the drugs against HIV in the brains:



$$\varepsilon_{\pi} = 1 - \left(\frac{1}{1 + \left(\frac{\pi D}{E D_{50}}\right)^m}\right).$$

Here a lower CPE score implies a lower concentration of the ART drug in the CSF. For our purposes, we consider a score of five to mean that a drug maintains equal effectiveness in the brain as it does in the plasma. Similarly, a minimum score of zero implies that the drug cannot penetrate through the BBB at all.

# 3 Model Analysis

For ease of notation we now define the following variables:

$$\Phi_b = \prod_{i=1}^n (1 - \varepsilon_i), \qquad \Phi_p = \prod_{i=1}^n (1 - \varepsilon_{PIi}), \text{ and}$$

$$\Phi_{\pi b} = \prod_{i=1}^n (1 - \varepsilon_{\pi i}), \qquad \Phi_{\pi p} = \prod_{i=1}^n (1 - \varepsilon_{\pi PIi}).$$

# 3.1 Model Feasibility

In view of (Smith 1996, Theorem 5.2.1), it follows that for any

$$(T_0, T_0^*, M_0, M_0^*, M_{B0}, M_{B0}^*, V_0, V_{B0}) \in \mathbb{R}_+^8,$$

system (1) has a unique local nonnegative solution

$$(T(t), T^*(t), M(t), M^*(t), M_B(t), M_R^*(t), V(t), V_B(t)) \in \mathbb{R}^8_+$$

through the initial value:

$$(T(0), T^*(0), M(0), M^*(0), M_B(0), M_B^*(0), V(0), V_B(0))$$
  
=  $(T_0, T_0^*, M_0, M_0^*, M_{B0}, M_{B0}^*, V_0, V_{B0}).$ 

Substituting

$$N(t) = T(t) + T^*(t) + M(t) + M^*(t) + M_B(t) + M_B^*(t)$$
 (2)

into system (1) leads to the following inequality

$$\frac{dN}{dt} = \lambda - (dT + \delta T^*) + \lambda_M - d_M(M + M_B) - \delta_M(M^* + M_B^*)$$



**105** Page 8 of 29 C. T. Barker et al.

$$\leq \lambda + \lambda_M - d_{\min}(T + T^* + M + M^* + M_B + M_B^*)$$
  
=  $\lambda + \lambda_M - d_{\min}N$ ,

where  $d_{\min} := \min\{d, \delta, d_M, \delta_M\}$ , and hence,

$$\limsup_{t \to \infty} N(t) \le \frac{\lambda + \lambda_M}{d_{\min}}.$$
 (3)

This implies that N(t) is ultimately bounded. Then from (2), T(t),  $T^*(t)$ , M(t),  $M^*(t)$ ,  $M_B(t)$  and  $M_B^*(t)$  are ultimately bounded due to the positivity of solutions. Then there exist  $t_0 > 0$  and  $\Lambda > 0$  such that

$$\Phi_p p T^*(t) + \Phi_p p_M M^*(t) \le \Lambda$$
 and  $\Phi_{\pi p} p_M M_B^*(t) \le \Lambda$ ,  $\forall t \ge t_0$ .

From the seventh and eighth equations of (1), we see that

$$\frac{dV}{dt} \leq \Lambda - cV, \ \forall \ t \geq t_0,$$

and

$$\frac{dV_B}{dt} \le \Lambda - cV_B, \ \forall \ t \ge t_0.$$

Thus,

$$\limsup_{t \to \infty} V(t) \le \frac{\Lambda}{c}, \text{ and } \limsup_{t \to \infty} V_B(t) \le \frac{\Lambda}{c}, \tag{4}$$

showing that V(t) and  $V_B(t)$  are ultimately bounded.

From the above discussion and Theorem 3.4.8 in Hale (1990), we have the following result:

**Theorem 1**  $\mathbb{R}^8_+$  is positively invariant for system (1) and system (1) admits a unique and bounded solution with the initial value in  $\mathbb{R}^8_+$ . Further, system (1) admits a connected global attractor on  $\mathbb{R}^8_+$ , which attracts all positive orbits in  $\mathbb{R}^8_+$ .

# 3.2 Basic Reproduction Number

We first determine the infection-free equilibrium,  $E_0$ , of system (1). To this end, we substitute  $T^* = M^* = M_B^* = 0$  into system (1), and we have  $V = V_B = 0$ . Furthermore, we arrive at the following systems:

$$\frac{dT}{dt} = \lambda - dT,\tag{5}$$



and

$$\begin{cases} \frac{dM}{dt} = \lambda_M - (\varphi + d_M)M + \psi M_B, \\ \frac{dM_B}{dt} = \varphi M - (\psi + d_M)M_B. \end{cases}$$
 (6)

It is easy to see that system (5) admits a unique positive equilibrium  $\hat{T} := \frac{\lambda}{d}$ , which is globally attractive in  $\mathbb{R}_+$ . We also see that

$$(\hat{M}, \hat{M}_B) = \left(\frac{\lambda_M a}{d_M}, \frac{\lambda_M (1 - a)}{d_M}\right) \tag{7}$$

is the unique positive equilibrium of system (6), where  $a = \frac{\psi + d_M}{\varphi + \psi + d_M}$ . Since system (6) is cooperative (see, e.g., Smith (1996)) and it admits a unique positive equilibrium  $(\hat{M}, \hat{M}_B)$ , we can show the global stability of  $(\hat{M}, \hat{M}_B)$  (see, e.g., Ji-Fa (1994)). The following results are concerned with the dynamics of systems (5) and (6).

# Lemma 2 The following statements are valid.

- (i) System (5) admits a unique positive equilibrium  $\hat{T} := \frac{\lambda}{d}$ , which is globally attractive in  $\mathbb{R}_+$ ;
- (ii) System (6) admits a unique positive equilibrium  $(\hat{M}, \hat{M}_B)$ , which is globally attractive in  $\mathbb{R}^2_+$ , i.e., for any  $(M(0), M_B(0)) \in \mathbb{R}^2_+$ , we have

$$\lim_{t\to\infty} (M(t), M_B(t)) = (\hat{M}, \hat{M}_B).$$

From the above discussions, the infection-free equilibrium of system (1) takes the form

$$E_0 = (T, T^*, M, M^*, M_B, M_B^*, V, V_B) = (\hat{T}, 0, \hat{M}, 0, \hat{M}_B, 0, 0, 0).$$

The equations for the infected cells and free virions in the plasma and the brain of the linearized system at the infection-free equilibrium,  $E_0$ , take the form

$$\begin{cases}
\frac{dT^*}{dt} = \Phi_b \beta \hat{T} V - \delta T^*, \\
\frac{dM^*}{dt} = \Phi_b \beta_M \hat{M} V + \psi M_B^* - (\varphi + \delta_M) M^*, \\
\frac{dM_B^*}{dt} = \Phi_{\pi b} \beta_M \hat{M}_B V_B + \varphi M^* - (\psi + \delta_M) M_B^*, \\
\frac{dV}{dt} = \Phi_p p T^* + \Phi_p p_M M^* - c V, \\
\frac{dV_B}{dt} = \Phi_{\pi p} p_M M_B^* - c V_B.
\end{cases} \tag{8}$$

The spectral bound or the stability modulus of an  $n \times n$  matrix  $\mathcal{M}$ , denoted by  $s(\mathcal{M})$ , is defined by

$$s(\mathcal{M}) := \max\{\text{Re}(\lambda) : \lambda \text{ is an eigenvalue of } \mathcal{M}\}.$$



**105** Page 10 of 29 C. T. Barker et al.

Motivated by (8), we define the following matrix:

$$J = \begin{pmatrix} -\delta & 0 & 0 & \Phi_b \beta \hat{T} & 0 \\ 0 & -(\varphi + \delta_M) & \psi & \Phi_b \beta_M \hat{M} & 0 \\ 0 & \varphi & -(\psi + \delta_M) & 0 & \Phi_{\pi b} \beta_M \hat{M}_B \\ \Phi_p p & \Phi_p p_M & 0 & -c & 0 \\ 0 & 0 & \Phi_{\pi p} p_M & 0 & -c \end{pmatrix}.$$
(9)

Clearly, J has non-negative off-diagonal elements, and J is irreducible (see a simple test on page 256 of Smith and Waltman (1995)). Then s(J) is a simple eigenvalue of J with a positive eigenvector (see, e.g., (Smith and Waltman 1995, Theorem A.5)).

We now use the next generation matrix method (Van den Driessche and Watmough 2002) to compute the basic reproduction number,  $\Re_0$ . We introduce the following matrices:

$$F = \begin{pmatrix} 0 & 0 & 0 & \Phi_b \beta \hat{T} & 0 \\ 0 & 0 & 0 & \Phi_b \beta_M \hat{M} & 0 \\ 0 & 0 & 0 & 0 & \Phi_{\pi b} \beta_M \hat{M}_B \\ \Phi_{p} p & \Phi_p p_M & 0 & 0 & 0 \\ 0 & 0 & \Phi_{\pi p} p_M & 0 & 0 \end{pmatrix}, \tag{10}$$

and

$$V = \begin{pmatrix} \delta & 0 & 0 & 0 & 0 \\ 0 & \varphi + \delta_M & -\psi & 0 & 0 \\ 0 & -\varphi & \psi + \delta_M & 0 & 0 \\ 0 & 0 & 0 & c & 0 \\ 0 & 0 & 0 & 0 & c \end{pmatrix}.$$
(11)

Note that J = F - V. The basic reproduction number corresponds to the spectral radius of  $FV^{-1}$ ,

$$\mathfrak{R}_0 = \rho(FV^{-1}).$$

The following is a general result showing that the local stability of the disease-free equilibrium,  $E_0$ , is determined by  $\mathfrak{R}_0$  (see, e.g. (Van den Driessche and Watmough 2002, Theorem 2)):

**Lemma 3** The following statements hold.

- (i)  $\Re_0 = 1$  if and only if s(J) = 0;
- (ii)  $\Re_0 > 1$  if and only if s(J) > 0;
- (iii)  $\Re_0 < 1$  if and only if s(J) < 0.

Thus, the disease-free equilibrium  $E_0$  is locally asymptotically stable if  $\mathfrak{R}_0 < 1$ , and unstable if  $\mathfrak{R}_0 > 1$ .



# 3.3 Threshold Dynamics

This subsection is devoted to studying the threshold dynamics of the system (1). Specifically, we will show that the basic reproduction number,  $\Re_0$ , is a threshold determining infection-free ( $\Re_0 < 1$ ) and infection-persistent ( $\Re_0 > 1$ ) dynamics. Let

$$\mathbf{X}_{0} = \{ (T_{0}, T_{0}^{*}, M_{0}, M_{0}^{*}, M_{B0}, M_{B0}^{*}, V_{0}, V_{B0}) \in \mathbb{R}_{+}^{8} : T_{0}^{*} > 0, M_{0}^{*} > 0, M_{B0}^{*} > 0, V_{0} > 0, V_{B0} > 0 \},$$

and

$$\partial \mathbf{X}_0 := \mathbb{R}^8_+ \backslash \mathbf{X}_0 = \{ (T_0, T_0^*, M_0, M_0^*, M_{B0}, M_{B0}^*, V_0, V_{B0}) \in \mathbb{R}^8_+ : T_0^* = 0 \text{ or } M_0^* = 0 \text{ or } M_{B0}^* = 0 \text{ or } V_0 = 0 \text{ or } V_{B0} = 0 \}.$$

We first prove the following lemma.

Lemma 4 Assume that

$$(T(t), T^*(t), M(t), M^*(t), M_B(t), M_B^*(t), V(t), V_B(t))$$

is a solution of the system (1) with initial value

$$(T(0), T^*(0), M(0), M^*(0), M_B(0), M_B^*(0), V(0), V_B(0)) \in \mathbb{R}^8_+.$$

Then the following statements hold:

(i) There exists a positive constant  $\zeta_0$  such that

$$\liminf_{t\to\infty} T(t) \geq \zeta_0, \quad \liminf_{t\to\infty} M(t) \geq \zeta_0, \quad \liminf_{t\to\infty} M_B(t) \geq \zeta_0;$$

(ii) If 
$$(T(0), T^*(0), M(0), M^*(0), M_B(0), M_B^*(0), V(0), V_B(0)) \in X_0$$
, then

$$T(t), T^*(t), M(t), M^*(t), M_B(t), M_B^*(t), V(t), V_B(t)) \gg 0, \ \forall \ t > 0.$$

## Proof

Part (i): In view of equation (4) or of Theorem 1 we see that there exists a  $\tilde{t}_0 > 0$  and a  $\xi > 0$  such that  $V(t) \leq \xi$  and  $V_B(t) \leq \xi$ ,  $\forall t \geq \tilde{t}_0$ . Then it follows from the first, third, and fifth equations in system (1) that

$$\frac{\mathrm{d}T}{\mathrm{d}t} \ge \lambda - [\Phi_b \beta \xi + d]T, \quad \forall t \ge \tilde{t}_0,$$

and

$$\begin{cases} \frac{\mathrm{d}M}{\mathrm{d}t} \geq \lambda_M - [\Phi_b \beta_M \xi + \varphi + d_M]M + \psi M_B, & \forall t \geq \tilde{t}_0, \\ \frac{\mathrm{d}M_B}{\mathrm{d}t} \geq \varphi M - [\psi + \Phi_{\pi b} \beta_M \xi + d_M]M_B, & \forall t \geq \tilde{t}_0. \end{cases}$$



**105** Page 12 of 29 C. T. Barker et al.

By the comparison principle, and similar arguments to those in Lemma 2, we see that

$$\liminf_{t\to\infty} T(t) \ge \frac{\lambda}{\Phi_b \beta \xi + d} \text{ and } \liminf_{t\to\infty} (M(t), M_B(t)) \ge (\underline{M}, \underline{M}_B),$$

where  $(\underline{M}, \underline{M}_B)$  is the unique root of the following algebraic equation:

$$\begin{cases} \lambda_M - [\Phi_b \beta_M \xi + \varphi + d_M] M + \psi M_B = 0, \\ \varphi M - [\psi + \Phi_{\pi b} \beta_M \xi + d_M] M_B = 0. \end{cases}$$

Thus, taking  $\zeta_0 = \min \left\{ \frac{\lambda}{\Phi_b \beta \xi + d}, \underline{M}, \underline{M}_B \right\}$ , Part (i) is proved.

Part (ii): In view of the first equation of system (1), it follows that

$$T(t) = e^{-\int_0^t b_1(s_1)ds_1} \left[ \int_0^t \lambda e^{\int_0^{s_2} b_1(s_1)ds_1} ds_2 + T(0) \right],$$

where

$$b_1(t) := d + \Phi_b \beta V(t).$$

Thus,  $T(t) > 0 \ \forall \ t > 0$ . From the third equation of system (1), it follows that

$$M(t) = e^{-\int_0^t b_2(s_1)ds_1} \left[ \int_0^t e^{\int_0^{s_2} b_2(s_1)ds_1} a_2(s_2)ds_2 + M(0) \right],$$

where

$$a_2(t) := \lambda_M + \psi M_R(t) > \lambda_M$$

and

$$b_2(t) := \Phi_b \beta_M V(t) + \varphi + d_M.$$

Thus,  $M(t) > 0 \,\forall t > 0$ . From the fifth equation of system (1), it follows that

$$M_B(t) = e^{-\int_0^t b_3(s_1)ds_1} \left[ \int_0^t e^{\int_0^{s_2} b_3(s_1)ds_1} a_3(s_2)ds_2 + M_B(0) \right],$$

where

$$a_3(t) := \varphi M(t) > 0,$$



and

$$b_3(t) := \psi + \Phi_{\pi b} \beta_M V_B(t) + d_M \ge \psi + d_M.$$

Thus,  $M_B(t) > 0 \ \forall t > 0$ . Next, we regard Theorem 4.1.1 of Smith (1996) as a generalized version to nonautonomous systems, and the irreducibility of the cooperative matrix

$$\begin{pmatrix} -\delta & 0 & 0 & \Phi_b \beta T(t) & 0 \\ 0 & -(\varphi + \delta_M) & \psi & \Phi_b \beta_M M(t) & 0 \\ 0 & \varphi & -(\psi + \delta_M) & 0 & \Phi_{\pi b} \beta_M M_B(t) \\ \Phi_p p & \Phi_p p_M & 0 & -c & 0 \\ 0 & 0 & \Phi_{\pi p} p_M & 0 & -c \end{pmatrix}$$
(12)

implies that

$$(T^*(t), M^*(t), M_R^*(t), V(t), V_B(t)) \gg 0, \ \forall \ t > 0.$$

This completes the proof.

We now establish the following theorem for the global threshold dynamics.

**Theorem 5** *The following statements hold.* 

- (i) If  $\Re_0 < 1$ , then the infection-free equilibrium  $E_0$  is globally attractive in  $\mathbb{R}^8_+$  for (1);
- (ii) If  $\Re_0 > 1$ , then system (1) is uniformly persistent with respect to  $(\mathbf{X}_0, \partial \mathbf{X}_0)$  in the sense that there is a positive constant  $\zeta > 0$  such that every solution

$$(T(t), T^*(t), M(t), M^*(t), M_B(t), M_B^*(t), V(t), V_B(t))$$

of (1) with

$$(T(0), T^*(0), M(0), M^*(0), M_B(0), M_B^*(0), V(0), V_B(0)) \in \mathbf{X}_0$$

satisfies

$$\liminf_{t\to\infty} u(t) \ge \zeta, \text{for each } u = T, \ T^*, \ M, \ M^*, \ M_B, \ M_B^*, \ V, \ V_B.$$
 (13)

Furthermore, system (1) admits at least one (componentwise) positive equilibrium.

**Proof** Part (i). Assume that  $\Re_0 < 1$ . It then follows from Lemma 3 (iii) that s(J) < 0. Thus, there exists a sufficiently small positive number  $\rho_0$  such that  $s(J_{\rho_0}) < 0$  (see,



**105** Page 14 of 29 C. T. Barker et al.

e.g., (Kato 2013, Section II.5.8)), where

$$J_{\rho_0} = \begin{pmatrix} -\delta & 0 & 0 & \Phi_b \beta(\hat{T} + \rho_0) & 0 \\ 0 & -(\varphi + \delta_M) & \psi & \Phi_b \beta_M(\hat{M} + \rho_0) & 0 \\ 0 & \varphi & -(\psi + \delta_M) & 0 & \Phi_{\pi b} \beta_M(\hat{M}_B + \rho_0) \\ \Phi_p p & \Phi_p p_M & 0 & -c & 0 \\ 0 & 0 & \Phi_{\pi p} p_M & 0 & -c \end{pmatrix}$$

has non-negative off-diagonal elements, and  $J_{\rho_0}$  is irreducible. From the first, third, and fifth equations of system (1), together with positivity of solutions, it follows that

$$\frac{dT}{dt} \le \lambda - dT,\tag{14}$$

and

$$\begin{cases}
\frac{dM}{dt} \le \lambda_M - (\varphi + d_M)M + \psi M_B, \\
\frac{dM_B}{dt} \le \varphi M - (\psi + d_M)M_B.
\end{cases}$$
(15)

By the comparison principle and Lemma 2, we get

$$\limsup_{t\to\infty} T(t) \leq \hat{T}, \ \limsup_{t\to\infty} (M(t), M_B(t)) \leq (\hat{M}, \hat{M}_B).$$

It follows that there is a  $t_1 > 0$  such that

$$T(t) \le \hat{T} + \rho_0, \ M(t) \le \hat{M} + \rho_0, \ M_B(t) \le \hat{M}_B + \rho_0, \ \forall \ t \ge t_1.$$
 (16)

In view of (16) and system (1), we see that

$$\begin{cases} \frac{dT^{*}}{dt} \leq \Phi_{b}\beta(\hat{T} + \rho_{0})V - \delta T^{*}, \ \forall \ t \geq t_{1}, \\ \frac{dM^{*}}{dt} \leq \Phi_{b}\beta_{M}(\hat{M} + \rho_{0})V + \psi M_{B}^{*} - (\varphi + \delta_{M})M^{*}, \ \forall \ t \geq t_{1}, \\ \frac{dM_{B}^{*}}{dt} \leq \Phi_{\pi b}\beta_{M}(\hat{M}_{B} + \rho_{0})V_{B} + \varphi M^{*} - (\psi + \delta_{M})M_{B}^{*}, \ \forall \ t \geq t_{1}, \\ \frac{dV}{dt} = \Phi_{p}pT^{*} + \Phi_{p}p_{M}M^{*} - cV, \ \forall \ t \geq t_{1}, \\ \frac{dV_{B}}{dt} = \Phi_{\pi p}p_{M}M_{B}^{*} - cV_{B}, \ \forall \ t \geq t_{1}. \end{cases}$$

$$(17)$$

Consider the following auxiliary system

$$\begin{cases} \frac{dT^*}{dt} = \Phi_b \beta(\hat{T} + \rho_0) V - \delta T^*, \ \forall \ t \geq t_1, \\ \frac{dM^*}{dt} = \Phi_b \beta_M (\hat{M} + \rho_0) V + \psi M_B^* - (\varphi + \delta_M) M^*, \ \forall \ t \geq t_1, \\ \frac{dM_B^*}{dt} = \Phi_{\pi b} \beta_M (\hat{M}_B + \rho_0) V_B + \varphi M^* - (\psi + \delta_M) M_B^*, \ \forall \ t \geq t_1, \\ \frac{dV}{dt} = \Phi_p p T^* + \Phi_p p_M M^* - c V, \ \forall \ t \geq t_1, \\ \frac{dV_B}{dt} = \Phi_{\pi p} p_M M_B^* - c V_B, \ \forall \ t \geq t_1. \end{cases}$$



(18)

Since  $J_{\rho_0}$  has non-negative off-diagonal elements and  $J_{\rho_0}$  is irreducible, it follows that  $s(J_{\rho_0})$  is simple and associates a strongly positive eigenvector  $\tilde{v} \in \mathbb{R}^5$  (see, e.g., (Smith and Waltman 1995, Theorem A.5)). For any solution  $(T(t), T^*(t), M(t), M^*(t), M_B(t), M_R^*(t), V(t), V_B(t))$  of (1) with nonnegative initial value

$$(T(0), T^*(0), M(0), M^*(0), M_B(0), M_B^*(0), V(0), V_B(0)),$$

there is a sufficiently large b > 0 such that

$$(T^*(t_1), M^*(t_1), M_R^*(t_1), V(t_1), V_B(t_1)) \le b\tilde{v}$$

holds. It is easy to see that  $U(t) := be^{s(J_{\rho_0}^0)(t-t_1)}\tilde{v}$  is a solution of (18) with  $U(t_1) := b\tilde{v}$ . By the comparison principle (Smith and Waltman 1995, Theorem B.1), it follows that

$$(T^*(t), M^*(t), M_R^*(t), V(t), V_B(t)) \le be^{s(J_{\rho_0})(t-t_1)} \tilde{v}, \ \forall \ t \ge t_1.$$

Since  $s(J_{\rho_0}) < 0$ , it follows that

$$\lim_{t \to \infty} (T^*(t), M^*(t), M_B^*(t), V(t), V_B(t)) = (0, 0, 0, 0, 0).$$

It then follows that the equations for T(t) and  $(M(t), M_B(t))$  in (1) are asymptotic to (5) and (6), respectively. By the theory for asymptotically autonomous semiflows (see, e.g., (Thieme 1992, Corollary 4.3)) and Lemma 2, it follows that

$$\lim_{t\to\infty} T(t) = \hat{T}, \ \lim_{t\to\infty} (M(t), M_B(t)) = (\hat{M}, \hat{M}_B).$$

Part (i) is proved.

Part (ii). Assume that  $\mathfrak{R}_0 > 1$ . It then follows from Lemma 3 (ii) that s(J) > 0. Suppose  $\Pi(t)P$  is the solution maps generated by system (1) with initial value P. By Theorem 1, we see that system  $\{\Pi(t)\}_{t\geq 0}$  admits a global attractor in  $\mathbb{R}^8_+$ . Now we prove that  $\{\Pi(t)\}_{t\geq 0}$  is uniformly persistent with respect to  $(\mathbf{X}_0, \partial \mathbf{X}_0)$ . By Lemma 4, it follows that both  $\mathbb{R}^8_+$  and  $\mathbf{X}_0$  are positively invariant. Clearly,  $\partial \mathbf{X}_0$  is relatively closed in  $\mathbb{R}^8_+$ .

Let  $M_{\partial} := \{P \in \partial \mathbf{X}_0 : \Pi(t)P \in \partial \mathbf{X}_0, \ \forall \ t \ge 0\}$  and  $\omega(P)$  be the omega limit set of the orbit  $O^+(P) := \{\Pi(t)P : t \ge 0\}$ . We next prove the following claims.

Claim 1:  $\omega(P) = \{E_0\}, \ \forall \ P \in M_{\partial}$ .

Since  $P \in M_{\partial}$ , we have  $\Pi(t)P \in M_{\partial}$ ,  $\forall t \geq 0$ . Next, we show that

$$(T^*(t), M^*(t), M_B^*(t), V(t), V_B(t)) = (0, 0, 0, 0, 0), \ \forall \ t > 0.$$
 (19)

Assume that (19) is not true. Then there exists  $\tau_0 > 0$  such that

$$(T^*(\tau_0), M^*(\tau_0), M_B^*(\tau_0), V(\tau_0), V_B(\tau_0)) \neq (0, 0, 0, 0, 0).$$



**105** Page 16 of 29 C. T. Barker et al.

Then the irreducibility of the cooperative matrix (12) implies that

$$(T^*(t), M^*(t), M_R^*(t), V(t), V_B(t)) \gg 0, \ \forall \ t > \tau_0,$$

which contradicts the fact that  $\Pi(t)P \in M_{\partial}$ ,  $\forall t \geq 0$ , and hence, (19) is true. By (19), it follows that the equations for T(t) and  $(M(t), M_B(t))$  in (1) satisfies (5) and (6), respectively. By Lemma 2, it follows that

$$\lim_{t\to\infty}T(t)=\hat{T},\ \lim_{t\to\infty}(M(t),M_B(t))=(\hat{M},\hat{M}_B).$$

Claim 1 is proved.

Since s(J) > 0, there exists a sufficiently small positive number  $\sigma_0$  such that  $s(J_{\sigma_0}) > 0$  (see, e.g., (Kato 2013, Section II.5.8)), where

$$J_{\sigma_0} = \begin{pmatrix} -\delta & 0 & 0 & \Phi_b \beta (\hat{T} - \sigma_0) & 0 \\ 0 & -(\varphi + \delta_M) & \psi & \Phi_b \beta_M (\hat{M} - \sigma_0) & 0 \\ 0 & \varphi & -(\psi + \delta_M) & 0 & \Phi_{\pi b} \beta_M (\hat{M}_B - \sigma_0) \\ \Phi_p p & \Phi_p p_M & 0 & -c & 0 \\ 0 & 0 & \Phi_{\pi p} p_M & 0 & -c \end{pmatrix}$$

has non-negative off-diagonal elements and  $J_{\sigma_0}$  is irreducible.

Claim 2:  $E_0$  is a uniform weak repeller for  $\Pi(t)$  in the sense that

$$\limsup_{t \to \infty} \|\Pi(t)P - E_0\| \ge \sigma_0, \ \forall \ P \in \mathbf{X}_0.$$

Suppose, by contradiction, there exists  $P_0 \in \mathbf{X}_0$  such that

$$\limsup_{t\to\infty} \|\Pi(t)P_0 - E_0\| < \sigma_0.$$

Thus, there exists  $t_2 > 0$  such that

$$T(t) \ge \hat{T} - \sigma_0, \ M(t) \ge \hat{M} - \sigma_0, \ M_B(t) \ge \hat{M}_B - \sigma_0, \ \forall \ t \ge t_2.$$
 (20)

In view of (20) and system (1), we see that

$$\begin{cases} \frac{dT^{*}}{dt} \geq \Phi_{b}\beta(\hat{T} - \sigma_{0})V - \delta T^{*}, \ \forall \ t \geq t_{2}, \\ \frac{dM^{*}}{dt} \geq \Phi_{b}\beta_{M}(\hat{M} - \sigma_{0})V + \psi M_{B}^{*} - (\varphi + \delta_{M})M^{*}, \ \forall \ t \geq t_{2}, \\ \frac{dM_{B}^{*}}{dt} \geq \Phi_{\pi b}\beta_{M}(\hat{M}_{B} - \sigma_{0})V_{B} + \varphi M^{*} - (\psi + \delta_{M})M_{B}^{*}, \ \forall \ t \geq t_{2}, \\ \frac{dV}{dt} = \Phi_{p}pT^{*} + \Phi_{p}p_{M}M^{*} - cV, \ \forall \ t \geq t_{2}, \\ \frac{dV_{B}}{dt} = \Phi_{\pi p}p_{M}M_{B}^{*} - cV_{B}, \ \forall \ t \geq t_{2}. \end{cases}$$
(21)



Consider the following auxiliary system

$$\begin{cases} \frac{dT^*}{dt} = \Phi_b \beta(\hat{T} - \sigma_0) V - \delta T^*, \ \forall \ t \ge t_2, \\ \frac{dM^*}{dt} = \Phi_b \beta_M (\hat{M} - \sigma_0) V + \psi M_B^* - (\varphi + \delta_M) M^*, \ \forall \ t \ge t_2, \\ \frac{dM_B^*}{dt} = \Phi_{\pi b} \beta_M (\hat{M}_B - \sigma_0) V_B + \varphi M^* - (\psi + \delta_M) M_B^*, \ \forall \ t \ge t_2, \\ \frac{dV}{dt} = \Phi_p p T^* + \Phi_p p_M M^* - c V, \ \forall \ t \ge t_2, \\ \frac{dV_B}{dt} = \Phi_{\pi p} p_M M_B^* - c V_B, \ \forall \ t \ge t_2. \end{cases}$$
(22)

Since  $J_{\sigma_0}$  is irreducible and has non-negative off-diagonal elements, it follows that  $s(J_{\sigma_0})$  is simple and associates a strongly positive eigenvector  $\tilde{u} \in \mathbb{R}^5$  (see, e.g., (Smith and Waltman 1995, Theorem A.5)). By Lemma 4, it follows that

$$(T^*(t_2), M^*(t_2), M_R^*(t_2), V(t_2), V_R(t_2)) \gg 0.$$

Thus, there is a positive number  $\varsigma > 0$  such that

$$(T^*(t_2), M^*(t_2), M_B^*(t_2), V(t_2), V_B(t_2)) \ge \zeta \tilde{u}$$

holds. It is easy to see that  $W(t) := \zeta e^{s(J_{\sigma_0})(t-t_2)}\tilde{u}$  is a solution of (22) with  $W(t_2) := \zeta \tilde{u}$ . By the comparison principle (Smith and Waltman 1995, Theorem B.1), it follows that

$$(T^*(t), M^*(t), M_R^*(t), V(t), V_B(t)) \ge \zeta e^{s(J_{\sigma_0})(t-t_2)} \tilde{u}, \ \forall \ t \ge t_2.$$

Since  $s(J_{\sigma_0}) > 0$ , it follows that

$$\lim_{t\to\infty} T^*(t) = \lim_{t\to\infty} M^*(t) = \lim_{t\to\infty} M_B^*(t) = \lim_{t\to\infty} V(t) = \lim_{t\to\infty} V_B(t) = \infty.$$

This contradiction proves the claim 2.

From the above claims, it follows that any forward orbit of  $\Pi(t)$  in  $M_{\partial}$  converges to  $E_0$  which is isolated in  $\mathbb{R}^8_+$  and  $W^s(E_0) \cap \mathbf{X}_0 = \emptyset$ , where  $W^s(E_0)$  is the stable set of  $E_0$  (see Smith and Zhao (2001)). It is obvious that there is no cycle in  $M_{\partial}$  from  $E_0$  to  $E_0$ . By (Thieme 1993, Theorem4.6) (see also (Zhao et al. 2003, Theorem 1.3.1) and (Hirsch et al. 2001, Theorem 4.3 and Remark 4.3)), we conclude that system (1) is uniformly persistent with respect to  $(\mathbf{X}_0, \partial \mathbf{X}_0)$  in the sense that there is a positive constant  $\zeta_1 > 0$  such that

$$\liminf_{t\to\infty} u(t) \geq \zeta_1, \ \forall u = T^*, \ M^*, \ M_B^*, \ V, \ V_B.$$

From Lemma 4 (i), we let  $\zeta := \min\{\zeta_0, \zeta_1\} > 0$ . Then it is easy to see that (13) holds. By (Zhao 1995, Theorem 2.4) (see also (Zhao et al. 2003, Theorem 1.3.7)), system (1) has at least one equilibrium

$$(\check{T},\check{T}^*,\check{M},\check{M}^*,\check{M}_B,\check{M}_B^*,\check{V},\check{V}_B)\in \mathbf{X}_0,$$



**105** Page 18 of 29 C. T. Barker et al.

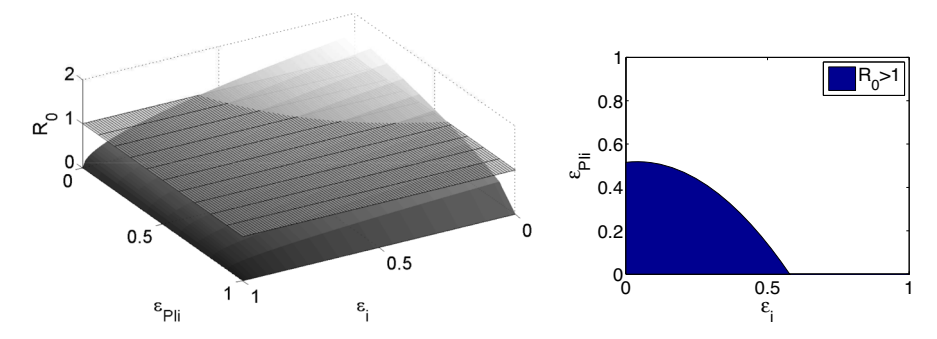


**Fig. 2** (Left) The reproduction number  $\mathfrak{R}_0$  depending on the effectiveness of PIs (x-axis) and RTIs (y-axis). The horizontal plane represents when  $\mathfrak{R}_0=1$ . (Right) The region in  $\varepsilon_i\varepsilon_{PIi}-space$  for  $\mathfrak{R}_0<1$  and  $\mathfrak{R}_0>1$ 

and hence,  $\check{T}^* > 0$ ,  $\check{M}^* > 0$ ,  $\check{M}^* > 0$ ,  $\check{V} > 0$ , and  $\check{V}_B > 0$ . Furthermore, we see that

$$\check{T} = \frac{\lambda}{\Phi_b \beta \check{V} + d},$$

and  $(\check{M}, \check{M}_B)$  satisfies

$$\begin{cases} \lambda_M - \Phi_b \beta_M \check{V} M - \varphi M + \psi M_B - d_M M = 0, \\ \varphi M - \psi M_B - \Phi_{\pi b} \beta_M \check{V}_B M_B - d_M M_B = 0, \end{cases}$$
(23)

From (23), it is not hard to see that  $\check{M} > 0$  and  $\check{M}_B > 0$ . Thus,

$$(\check{T},\check{T}^*,\check{M},\check{M}^*,\check{M}_B,\check{M}_B^*,\check{V},\check{V}_B)$$

is a (componentwise) positive equilibrium of system (1). This completes the proof of Part (ii).

Theorem 5 indicates that the basic reproduction number,  $\mathfrak{R}_0$ , is a critical threshold, which allows us to determine whether the infection is avoided ( $\mathfrak{R}_0 < 1$ ) or persists ( $\mathfrak{R}_0 > 1$ ) in the brain. As the threshold,  $\mathfrak{R}_0$ , is the function of control parameters, such as pre-exposure prophylaxis, the established threshold condition allows us to identify the strength of such treatment required to avoid the infection. In Fig. 2, we present how the value of  $\mathfrak{R}_0$  changes based on the drug efficacies  $\varepsilon_i$  and  $\varepsilon_{PIi}$ . Moreover, we also identified the region in  $\varepsilon_i \varepsilon_{PIi}$ -space, in which  $\mathfrak{R}_0 < 1$ , asserting the infection control threshold.

## **4 Numerical Simulations**

In this section, we present the numerical simulations of the plasma viral load (PVL) and the brain viral load (BVL) under different treatment protocols. Consistent with the



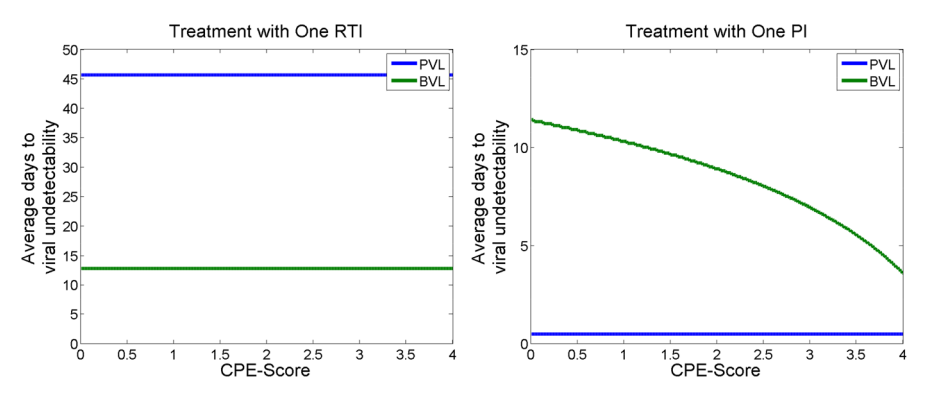


**Fig. 3** The average time the viral loads in the plasma (blue) and the brain (green) become undetectable depending on the mean CPE score of the ART regimen with either a single RTI (left) or PI (right) (Color figure online)

analytical result established in Theorem 5, we observed that our numerical simulations of viral loads dynamics converge to the infection-free steady state or infected steady state depending upon the choice of drug efficacies from the white  $(\Re_0 < 1)$  or blue  $(\Re_0 > 1)$  regions, respectively, shown in Fig. 2 (right). Since there is no known cure for HIV rather than viral elimination, an undetectable viral load is a marked success for current treatment protocols. Therefore, we take the time for the viral load to be undetectable as the index for the treatment evaluation. For all simulations, we consider a detectable viral load to be 50 copies of viral RNA per mL of blood plasma, the standard lower limit to measure HIV according to current assays (aidsinfo 2018).

We consider how the different protocols affect the time the viral loads take to reach undetectable levels. We first examine whether the CPE score alters the treatment time for the viral load to become undetectable in the plasma and the brain. Next, we explore how the slope of the dose-response curve affects the time for viral undetectability. Then, we analyze the effect of the number of drugs in a given ART regimen. Finally, we examine if the treatment initiation time affects the average time for the PVL and BVL to fall below the detectable level.

#### 4.1 Effect of the CPE Score

To better understand the effect of the CPE score on the overall treatment of HIV, we considered its effect on the time that the PVL and the BVL reduce to undetectable levels in the presence of constant drug levels. In Fig. 3, we show the average time the viral loads in the brain and the plasma become undetectable depending on the CPE score of an ART regimen with a single drug. Treatment was initiated after a steady state viral load was achieved ( $\sim$ 250 dpi), and we considered a single RTI (Fig. 3, left) and a single PI (Fig. 3, right).

We observe that the CPE score has a negligible effect on the plasma viral load, as the average number of days for the PVL to become undetectable remains constant despite the CPE score or the drug type (RTI or PI). However, even with one drug present, we observe that the CPE score affects the number of days to viral undetectability for a PI



**105** Page 20 of 29 C. T. Barker et al.

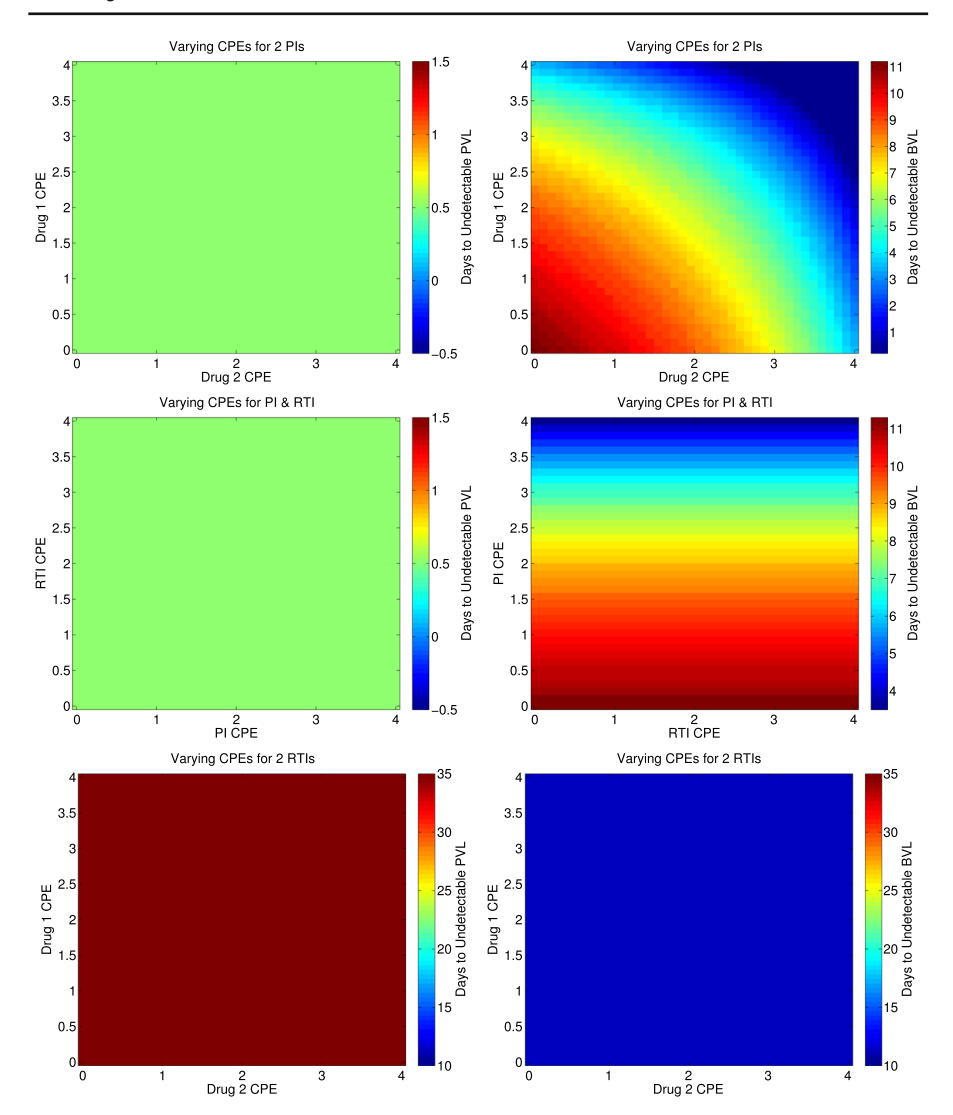


**Fig. 4** Average days to viral undetectability in the PVL (left column) and BVL (right column) depending on the CPE scores for two PIs (top row), two RTIs (bottom row) and a combination of one RTI and one PI (middle row). We used different color scales for different figures as appropriate for visibility purposes

differently than it does for an RTI. In particular, as the CPE score increases for a PI, the number of days for the BVL to reach undetectable levels decreases ( $\sim 10$  days vs.  $\sim 3$  days). There is no observed effect of the CPE score and the BVL if an ART protocol includes only a single RTI. Hence, the BBB affects single-drug protocols with PIs more than RTIs.

We next analyzed the effect of the CPE score under the ART regimen with two drugs. We considered two PIs, two RTIs, or a combination of one PI and one RTI. We present the simulated number of days to viral undetectability in the PVL (Fig. 4,



left column) and BVL (Fig. 4, right column). Similar to the treatments with a single drug, we observe no discernible effect of the CPE score on the PVL with two drugs. However, we observe a strong effect of the CPE score on the days for which the BVL becomes undetectable in the presence of two drugs. For ART with two PIs, we see that as the CPE increases for either drug, the days to viral clearance decrease (~ 9 days vs. ~ 1 day). Furthermore, if ART includes an RTI and a PI, we note that as the CPE score increases for the PI, the time to undetectable BVL decreases; however, the CPE score for the RTI shows a negligible effect on the time to the undetectability of BVL. In fact, if treatment includes only two RTIs, we do not observe any noticeable effect of the CPE score on time to viral undetectability. These results combined suggest that PIs with higher CPE scores should be considered more than RTIs to control HIV in the brain better.

# 4.2 Effect of the Slope of the dose-response Curve

We used our model (1) to explore the influence of the slope of the dose-response curve on the time viral RNA becomes undetectable. We first considered treatment with one drug. Based on experimental evidence (Shen 2008), we considered any drug whose slope, m, is greater than 1.9 to be a PI, while a drug with  $m \le 1.9$  is considered to be an RTI (Table 2). We present the results on time to viral undetectability with a single drug of a low CPE score (CPE= 1; Fig. 5, left) and a high CPE score (CPE= 4; Fig. 5, right) for the slope of the dose-response curve from 0 to 5. As mentioned before, the treatment was initiated after a steady-state viral load was achieved in the brain and the plasma ( $\sim$ 250 dpi).

We observe that if  $m \le 1.9$  (RTI), then the PVL becomes undetectable after about only 40 days, whereas if m > 1.9 (PI), then the PVL reaches the undetectable level within a single day. The number of days the BVL takes to reach the undetectable level also decreases as the slope of the dose-response curve increases; however, this reduction is significantly less than that observed in the PVL ( $\sim 40$  days less in PVL compared to  $\sim 6$  days less in BVL). Interestingly, for low slopes that correspond to an RTI, we note that the PVL becomes undetectable several weeks after the BVL becomes undetectable and that this behavior switches for the slope corresponding to a PI (Fig. 5). This switch occurs regardless of the drug's CPE score, reinforcing the previous section's observation that RTIs are less effective for the PVL.

To examine the effect of the slope of the dose-response curve further, we considered the ART regimen of two drugs, including both RTI and PI. We considered combinations of RTIs and PIs of both high and low CPE scores and computed the time to undetectability of PVL. Our simulations show that in all regimens considered, neither the BVL nor the PVL has any noticeable difference in the time to undetectability, suggesting that once multiple drugs are present in the ART regimen, the slope of the dose-response curve has less effect on the time to viral undetectability (See Supplemental Information). For ART with two drugs, even if the slopes of the dose-response curves are low, the average number of days to viral undetectability is much less than the regimen with one drug ( $\sim$  10 days in two drugs compared to  $\sim$  40 days in one



**Table 2** Parameters related to drug pharmacodynamics and CPE scores. Note that  $\Phi_j$  represents the residual viral infection (production) rate for FIs, IIs, and RTIs (PIs) and  $\varepsilon_j = 1 - \Phi_j$  represents the drug's efficacy

Drug Type	Drug Name	Drug Abbreviation	Drug CPE Score (according to Letendre, 2011[31])	Inhibitory Quotient (Davg/IC50)	Hill's coefficient m <sub>i</sub>	$\Phi_j$	E j
NRTI	Abacavir	ABC	3	50.9	0.95	0.023353685	0.976646315
	Didanosine	lpp	2	2.4	1.07	0.281556981	0.718443019
	Emtricitabine	FTC	3	226.9	1.18	0.001657276	0.998342724
	Lamivudine	3TC	2	101.4	1.15	0.004908169	0.995091831
	Stavudine	d4T	2	0.85	1.13	0.545782997	0.454217003
	Tenofovir	TDF	1	2.7	76.0	0.276187136	0.723812864
	Zalcitabine	ddC	1	Not included	Not included	Not calculated	not calculated
	Zidovudine	AZT	4	2.4	0.85	0.322097664	0.677902336
NNRTI	Delavirdine	DLV	3	101.2	1.56	0.000744038	0.999255962
	Efavirenz	EFV	3	1042.5	1.69	7.93319E-6	0.9999992067
	Etravirine	TMC125	2	203.4	1.81	6.63523E-5	0.999933648
	Nevirapine	NVP	4	195.6	1.55	0.000280709	0.99719291
PI	Atazanavir	ATV	2	199.8	2.69	6.47736E-7	0.999999352
	Darunavir/r	DRV	3	410.6	3.61	3.67754E-10	1
	Fosamprenavir	APV	2	39.7	2.09	0.000455334	0.999544666
	Indinavir	IDV	3	09	4.53	8.80998E-9	0.9999999991
	Lopinavir/r	LPV	3	343.2	2.05	6.34053E-6	0.999993659
	Nelfinavir	NFV	1	21.5	1.81	0.003860172	0.996139828
	Saquinavir	SQV	-	120	3.65	2.57625E-8	0.999999974
	Tipranavir/r	tPV	1	244.5	2.51	1.01256E-6	0.999998987
FI	Enfuvirtide	T20	1	25.1	1.65	0.004879933	0.995120067
П	Raltegravir	RAL	3	8.68	1.1	0.007052165	0.992947835



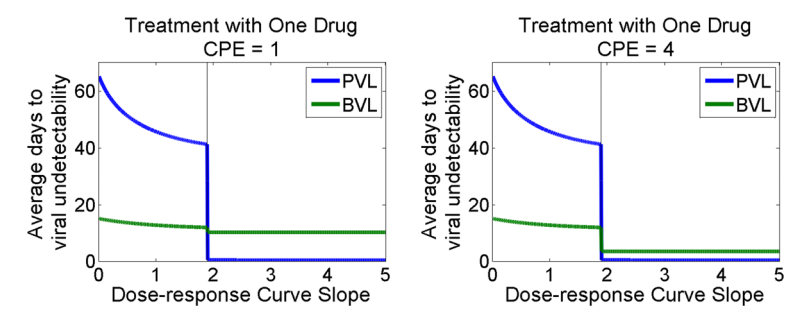


Fig. 5 Simulated number of days for the viral load in the plasma (blue) and in the brain (green) to become undetectable depending on the slope of the dose-response curve for ART regimen with a single drug of a CPE score of one (left) and four (right). Here, a dose-response slope greater than 1.9 (represented by the vertical line) corresponds to a PI, while a dose-response slope less than 1.9 corresponds to an RTI. The vertical lines separate the type of drugs based on this slope value

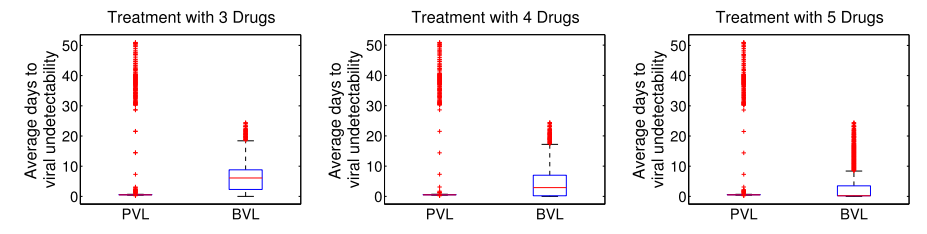


Fig. 6 Box plots showing the time for the virus to become undetectable (in days) depending on the number of drugs in an ART regimen. For each case, 15000 samples of drug were randomly generated by choosing the drug-response slope between zero and five and the CPE score between zero and five

drug). In particular, we observe that if both an RTI and a PI are present in ART, the BVL reaches undetected levels at least three days after the PVL becomes undetectable.

## 4.3 Effect of Multiple Drugs

In the previous section, our model predictions showed that more than one drug in ART regimens led to less time for the virus to become undetectable. Here we sought to examine whether this correlation remains the same for ART regimens with three or more drugs. For our computations, we randomly selected the sample of 15000 combinations of drugs in each of 3-, 4-, and 5-drug regimens by choosing the uniformly distributed drug-response slope between zero and five and the uniformly distributed CPE score between zero and five. Drug types were categorized by the slope of the dose-response curve selected as follows: RTI if  $m \le 1.9$  and PI if m > 1.9. Again, the drug concentration was assumed to be constant, and the treatment was initiated after the viral load reached a steady-state ( $\sim 250$  dpi).

In many cases (Fig. 6), we observed that ART regimens with multiple drugs reduce the PVL to the undetectable level before the BVL. However, many outliers appeared in our samples among the PVL, implying more uncertainty in PVL outcomes. This is likely because we chose uniformly distributed random slopes between 0 and 5, which



**105** Page 24 of 29 C. T. Barker et al.

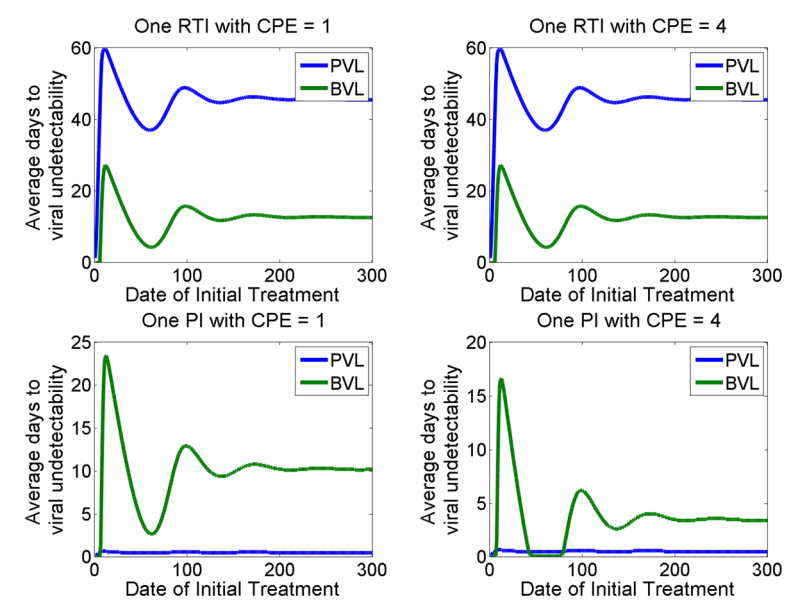


**Fig. 7** The time (in days) for the viral load to become undetectable in the plasma (blue) and the brain (green) depending on the treatment initiation time of one RTI (top row) and one PI (bottom row) with a low CPE score (left column) and a high CPE score (right column)

increases the likelihood of selecting slopes corresponding to PIs (1.9 < m < 5) than RTIs  $(0 < m \le 1.9)$ .

Note that the number of drugs in a treatment regimen highly affects the time for the BVL to become undetectable. Specifically, the median days for the BVL to become undetectable decreases from  $\sim 7$  days for three drugs to  $\sim 0.5$  days for five drugs. We also observed that viral suppression in the plasma might not imply viral suppression in the brain for drug regimens with a higher number of drugs. This result highlights the role of the BBB, impacting the permeability of many drugs in regimens with multiple drugs.

#### 4.4 Effect of Treatment Initiation Time

In Fig. 7, we present the predicted time in days post-infection that the plasma and brain viral load achieve undetectable levels depending on the treatment initiation time. We performed computations using a single RTI or PI with a corresponding CPE score of either one or four. The time of treatment initiation was varied between one day and 300 days post-infection (dpi).

We observed that the earliest initiated treatment (< 3 dpi) is more effective as it can prevent infection from reaching detectable viral levels in the brain. The effectiveness of early treatment revealed in our results is consistent with previous studies (Chun and Engel 1998; Vaidya and Rong 2017). Furthermore, our simulations suggest that, in general, the time for the PVL and BVL to reach undetectable levels varies significantly



within the first 100 days post-infection. For instance, if treatment begins during the second-week post-infection, the virus is detectable in both the plasma and the brain for longer (15-20 dpi) than for any other treatment initiation time. If the treatment is initiated between eight and ten weeks post-infection, the time to viral undetectability (<5 dpi in the brain,  $\sim$  8 dpi in the plasma) is significantly less than other treatment initiation times. Once the steady state is reached, the treatment initiation time does not affect the time for the virus to fall below undetectable levels.

We also compared the outcome of PIs and RTIs for varying treatment initiation times. We found that treatment with a PI is highly effective at reducing the PVL but less effective at reducing the BVL. In contrast, treatment with an RTI reduces the BVL consistently more efficiently than the PVL. In some cases with high CPE scores, the treatment initiation time may result in the BVL becoming undetectable faster than the PVL. However, in treatment with a low CPE score, we did not observe such a case in which the BVL becomes undetectable before the PVL.

## 5 Discussion

Despite the success of ART in controlling HIV, a cure remains beyond the scope of current treatment, mainly due to the formation of viral reservoirs, such as the brain. In particular, the effect of the BBB, which blocks the drugs from entering the brain, remains a challenge for developing proper treatment protocols. A comprehensive look at the infection of HIV in the brain and the effect the BBB poses on ART has not been explored in previous studies.

The main objective of this study was to develop a mathematical model to investigate the impact of BBB on treatment-mediated viral suppression in the brain. Our model provides new insights that may help mitigate HIV from the brain. A critical finding from the model simulations is that the CPE score plays a significant role in the viral suppression in the brain for drugs with high slopes (m > 1.9), compared to drugs with low slopes (m < 1.9). A more significant suppression with a high-slope drug indicates that the protease inhibitors are more effective because, generally, ART drugs with larger slopes (m > 1.89) tend to be protease inhibitors (aidsinfo 2018) (see Table 2). As expected, our predictions suggest that changing the CPE score does not affect the time for the PVL to become undetectable for either drug type; however, the CPE score significantly impacts the time for the BVL to reach undetectable levels. Particularly for PIs, a higher CPE score corresponds to a shorter time for the BVL to become undetectable. For the drugs with low slopes, the CPE score has a negligible impact on the time to viral undetectability in the brain. A similar phenomenon was observed when we considered ART with two drugs. PIs, which often have a higher CPE score, generally manage to enter the brain with a higher percentage of drugs, resulting in a lower time to the BVL undetectability. Our simulations are also supported by the results of Letendre (2011), which illustrate the lower impact of the BBB on PI treatments to control HIV in the brain.

We further considered the effect the BBB has on drug regimens with higher dose-response curve slopes than those with lower slopes. In this case, we found that the PVL reached undetectable levels in significantly less time ( $\approx 50$  days vs.  $\approx 1$  day) if the



slope of the dose-response curve of a drug is over 1.9, independent of the CPE score. This drastic difference in reduction time for PIs was not observed in the case of BVL. However, the BVL becomes undetectable roughly three weeks before the PVL for ART with lower slopes, unlike the results from ART with higher slopes. Furthermore, our simulations suggest that the BBB reduces the effect of ART on controlling HIV in the brain, especially for drugs with higher slopes. Therefore, depending on the slope of the dose-response curves, control of the PVL may not necessarily indicate control of the BVL.

The time for the viral load to reach undetectable levels depends on the treatment initiation time. While an early treatment may prevent the establishment of a viral reservoir, as demonstrated in previous studies (Archin et al. 2012), our model suggests that for the treatment initiated after three dpi, early ART may not always result in a shorter time for viral undetectability. For example, the treatment initiated during the second-week post-infection (10-14 dpi) may take longer for the viral load to become undetectable than the treatment begun at 60 dpi (Fig. 7). We used our model to formulate the basic reproduction number,  $\Re_0$ , which we prove (Theorem 5) to provide a threshold condition for the global stability of the infection-free equilibrium ( $\Re_0 < 1$ ) or persistence of infection ( $\Re_0 > 1$ ) in the brain. Based on this formulation, we can compute the combination of ART drugs that asserts  $\Re_0 < 1$  to avoid infection.

We acknowledge several limitations of this study. We are unable to present the model fitting to the realistic viral dynamics data because of its unavailability. However, we would like to note that our model is based on experimental evidence on realistic HIV dynamics. Without treatment, this model has been carefully developed based on solid biological evidence and validated using experimental data from SIV/SHIV-infected macaques in a previous study (Barker and Vaidya 2020). We only studied constant treatment, often leading to viral eradication. In reality, maintaining a constant drug concentration is less likely, and so far, no evidence of consistent viral eradication has occurred. Time-varying drug concentration may be necessary, as done previously (Duwal et al. 2019; Vaidya and Rong 2017), to model a more-likely scenario.

The study by Vaidya and Rong (2017) suggests that the pharmacodynamics of each drug play a critical role in the control of infection. They also found that the basic reproduction number may not be the most reasonable indicator of infection persistence. They suggested the infection invasion threshold incorporating time-dependent drug concentration for more accurate criteria for infection control. We did not take into account the drug resistance nor the potential for viral mutation, which could result in viral rebound even amid treatment. A previous study (Strazielle et al. 2016) suggests that astrocytes and T-cells may harbor viral RNA in the brain, neither of which was considered in our model. Explaining drug concentration in the CSF entirely based on CPE score may also have some limitations; experiments analyzing more detailed drug concentrations may provide a better drug profile in the CSF. While these theoretical results offer insight into potential ART treatment improvements, they must be tested by *in vitro* and *in vivo* experiments before any recommendations can be offered in practice.

A similarly structured model may be utilized for each viral reservoir, contributing to viral rebound. This study did not include the presence of latently-infected cells and reservoirs, which are known to contribute to viral rebound (Ho and Shan 2013)



significantly. While our study provides a great insight into the brain virus contributing to the HIV reservoir, more complex models with all potential reservoirs in combination can provide a complete picture of potential HIV eradication through early treatments. However, such models need data with all the reservoirs collected simultaneously.

In summary, the model developed in this study underscores the role of BBB in the altered effectiveness of ART on viral control in the brain. The BBB-impacted CPE scores, the dose-response slope, the number of drugs in an ART regimen, and the treatment initiation time are the essential factors that must be considered to design the ideal treatment protocol for mitigating HIV in the brain. All these results combined indicate that the choice of drugs in the treatment regimens is vital for successfully controlling the virus in the brain.

Acknowledgements This work was supported by NSF grants DMS-1616299 (NKV), DMS-1836647 (NKV), and DEB- 2030479 (NKV) from National Science Foundation, United States, and UGP award (NKV) from San Diego State University. The research of F.-B. Wang was supported in part by the Ministry of Science and Technology, Taiwan, the National Center for Theoretical Sciences, National Taiwan University, and Chang Gung Memorial Hospital (BMRPD18 and NMRPD5M0021). NKV would like to thank National Center for Theoretical Sciences for supporting the NCTS visit, during which some of the work was carried out.

**Data Availibility** All data generated or analyzed during this study are included in this published article.

### **Declarations**

Conflicts of interest Authors declare NO conflict of interest.

## References

Abreu CM, Veenhuis RT, Avalos CR, Shelby G, Queen SE, Shirk EN, Bullock BT, Ming L, Metcalf PKA, Beck SE, Mangus LM, Mankowski JL, Clements JE, Lucio G (2019) Infectious virus persists in cd4+ t cells and macrophages in antiretroviral therapy-suppressed simian immunodeficiency virus-infected macaques. J Virol 93(15):10–1128

Archin NM, Vaidya NK, Kuruc JD, Liberty AL, Ann W, Kearney MF, Cohen MS, Coffin JM, Bosch RJ, Gay CL et al (2012) Immediate antiviral therapy appears to restrict resting cd4+ cell hiv-1 infection without accelerating the decay of latent infection. Proc Natl Acad Sci 109(24):9523–9528

Ash MK, Lena A-H, Schneider JR (2021) Hiv in the brain: Identifying viral reservoirs and addressing the challenges of an HIV cure. Vaccines 9(8):867

Barker CT, Vaidya NK (2020) Modeling hiv-1 infection in the brain. PLoS Comput Biol 16(11):e1008305 Bates DM, Watts DG (1988) Nonlinear regression analysis and its applications, vol 2. Wiley, New York

Bednar MM, Buckheit SC, Tompkins LA, Twigg AK, Elena D, Kincer LP, Ronald S (2015) Compartmentalization, viral evolution, and viral latency of HIV in the CNS. Curr HIV/AIDS Rep 12(2):262–271

Beguelin C, Vázquez M, Bertschi M, Yerly S, de Jong D, Gutbrod K, Rauch A, Cusini A (2016) Viral escape in the central nervous system with multidrug-resistant human immunodeficiency virus-1, Open forum infectious diseases, vol 3. Oxford University Press

Boffito M, Back DJ, Blaschke TF, Rowland M, Bertz RJ, Gerber JG, Miller V (2003) Protein binding in antiretroviral therapies. AIDS Res Hum Retroviruses 19(9):825–835

Callaway DS, Perelson AS (2002) Hiv-1 infection and low steady state viral loads. Bull Math Biol 64(1):29–64

Chun T-W, Engel DM, Berrey M, Shea T, Corey L, Fauci AS (1998) Early establishment of a pool of latently infected, resting cd4+ t cells during primary hiv-1 infection. Proc Natl Acad Sci 95(15):8869–8873



Clements JE, Tahar B, Mankowski JL, Suryanarayana K, Michael P Jr, Tarwater PM, Lifson JD, Christine ZM (2022) The central nervous system as a reservoir for simian immunodeficiency virus (siv): steady-state levels of siv dna in brain from acute through asymptomatic infection

- David PC (1988) HIV persistence in monocytes leads to pathogenesis and aids1. Cell Immunol 112(2):414–424
- Fois AF, Brew BJ (2015) The potential of the CNS as a reservoir for HIV-1 infection: implications for HIV eradication. Curr HIV/AIDS Rep 12(2):299–303
- Gray LR, Roche M, Flynn JK, Wesselingh SL, Gorry PR, Churchill MJ (2014) Is the central nervous system a reservoir of HIV-1? Curr Opin HIV AIDS 9(6):552
- Guidelines for the use of antiretroviral agents in adults and adolescents living with hiv. Accessed June 18, 2018, https://aidsinfo.nih.gov/guidelines/html/1/adult-and-adolescent-arv/458/plasma-hiv-1-rna--viral-load--and-cd4-count-monitoring
- Hal S, Qiang ZX (2001) Robust persistence for semidynamical systems. Nonlinear Anal Theory Methods Appl 47(9):6169–6179
- Hale J (1990) Asymptotic behavior of dissipative systems. Bull Am Math Soc 22:175-183
- Haney AF, Muscato JJ, Brice Weinberg J (1981) Peritoneal fluid cell populations in infertility patients. Fertil Steril 35(6):696–698
- Herwig K, Ruth B-W, Michael S (2012) Macrophages and their relevance in human immunodeficiency virus type i infection. Retrovirology 9(1):82
- Hirsch MW, Smith HL, Xiao-Qiang Z (2001) Chain transitivity, attractivity, and strong repellors for semidynamical systems. J Dyn Differ Equ 13(1):107–131
- Ho Y-C, Shan L, Hosmane NN, Wang J, Laskey SB, Rosenbloom DIS, Lai J, Blankson JN, Siliciano JD, Siliciano RF (2013) Replication-competent noninduced proviruses in the latent reservoir increase barrier to hiv-1 cure. Cell 155(3):540–551
- Huang Y, Zhang C, Jianhong W, Lou J (2017) Modelling the hiv persistence through the network of lymphocyte recirculation in vivo. Infect Disease Modell 2(1):90–99
- Ji-Fa J (1994) On the global stability of cooperative systems. Bull Lond Math Soc 26(5):455–458
- Joanna H, Victor V, Serena S (2015) Cns reservoirs for hiv: implications for eradication. J Virus Eradicat 1(2):67
- Kato T (2013) Perturbation theory for linear operators, vol 132. Springer Science & Business Media
- Kepler TB, Perelson AS (1998) Drug concentration heterogeneity facilitates the evolution of drug resistance. Proc Natl Acad Sci 95(20):11514–11519
- Kincer LP, Joseph SB, Gilleece MM, Hauser BM, Sizemore S, Zhou S, Di Germanio C, Zetterberg H, Fuchs D, Deeks SG, et al (2023) Rebound hiv-1 in cerebrospinal fluid after antiviral therapy interruption is mainly clonally amplified r5 t cell-tropic virus. Nat Microbiol, pp 1–12
- Kumar R, Torres C, Yamamura Y, Rodriguez I, Martinez M, Staprans S, Donahoe RM, Kraiselburd E, Stephens EB, Kumar A (2004) Modulation by morphine of viral set point in rhesus macaques infected with simian immunodeficiency virus and simian-human immunodeficiency virus. J Virol 78(20):11425–11428
- Letendre S (2011) Central nervous system complications in hiv disease: Hiv-associated neurocognitive disorder. Topics Antiviral Med 19(4):137
- Max K, von Menz S, Huisinga W (2010) Drug-class specific impact of antivirals on the reproductive capacity of hiv. PLoS Comput Biol 6(3):1000720
- Michael L, Christine H, Michael DM, Arlene H, Viviana S, James R, Nancy R, Scott B, Eugene S, Perelson Alan S et al (2003) Determining the relative efficacy of highly active antiretroviral therapy. J Infect Dis 187(6):896–900
- Nath A (2015) Eradication of human immunodeficiency virus from brain reservoirs. J Neurovirol 21(3):227–234
- Osborne O, Peyravian N, Nair M, Daunert S, Toborek M (2020) The paradox of hiv blood-brain barrier penetrance and antiretroviral drug delivery deficiencies. Trends Neurosci 43(9):695–708
- Prinz M, Priller J (2014) Microglia and brain macrophages in the molecular age: from origin to neuropsychiatric disease. Nat Rev Neurosci 15(5):300–312
- Ramratnam B, Bonhoeffer S, Binley J, Hurley A, Zhang L, Mittler JE, Markowitz M, Moore JP, Perelson AS, Ho DD (1999) Rapid production and clearance of hiv-1 and hepatitis c virus assessed by large volume plasma apheresis. The Lancet 354(9192):1782–1785
- Roda WC, Li MY, Akinwumi MS, Asahchop EL, Gelman BB, Witwer KW, Christopher P (2017) Modeling brain lentiviral infections during antiretroviral therapy in aids. J Neurovirol 23(4):577–586



- Rosenbloom DIS, Hill AL, Alireza Rabi S, Siliciano RF, Nowak MA (2012) Antiretroviral dynamics determines HIV evolution and predicts therapy outcome. Nat Med 18(9):1378–1385
- Schnell G, Joseph S, Spudich S, Price RW, Swanstrom R (2011) Hiv-1 replication in the central nervous system occurs in two distinct cell types. PLoS Pathogens 7(10)
- Schwartz EJ, Vaidya NK, Dorman KS, Susan C, Mealey RH (2018) Dynamics of lentiviral infection in vivo in the absence of adaptive immune responses. Virology 513:108–113
- Shen L, Peterson AR, Sedaghat S, McMahon MA, Callender M, Zhang H, Zhou Y, Pitt E, Anderson KS, Acosta EP et al (2008) Dose-response curve slope sets class-specific limits on inhibitory potential of anti-hiv drugs. Nat Med 14:762–766
- Smith Hal L (1996) Monotone dynamical systems: an introduction to the theory of competitive and cooperative systems. Bull Am Math Soc 33:203–209
- Smith HL, Waltman Paul (1995) The theory of the chemostat: dynamics of microbial competition, vol 13. Cambridge University Press
- Stafford MA, Lawrence C, Yunzhen C, Daar Eric S, Ho DD, Perelson AS (2000) Modeling plasma virus concentration during primary hiv infection. J Theor Biol 203(3):285–301
- Strazielle N, Creidy R, Malcus C, Boucraut J, Ghersi-Egea J-F (2016) T-lymphocytes traffic into the brain across the blood-csf barrier: evidence using a reconstituted choroid plexus epithelium. PLoS One 11(3)
- Sulav D, Laura D, Saye K, Max K, von, (2019) Mechanistic framework predicts drug-class specific utility of antiretrovirals for hiv prophylaxis. PLoS Comput Biol 15(1):e1006740
- The centers for disease control and prevention. Accessed May 5, 2019. https://www.cdc.gov/hiv/basics/statistics.html
- The joint united nations programme on hiv and aids. Accessed August 23, 2019. https://www.unaids.org/en/resources/fact-sheet
- Thieme HR (1992) Convergence results and a poincaré-bendixson trichotomy for asymptotically autonomous differential equations. J Math Biol 30(7):755–763
- Thieme HR (1993) Persistence under relaxed point-dissipativity (with application to an endemic model). SIAM J Math Anal 24(2):407–435
- Vaidya NK, Libin R (2017) Modeling pharmacodynamics on hiv latent infection: choice of drugs is key to successful cure via early therapy. SIAM J Appl Math 77(5):1781–1804
- Vaidya NK, Ribeiro RM, Miller CJ, Perelson AS (2010) Viral dynamics during primary simian immunod-eficiency virus infection: effect of time-dependent virus infectivity. J Virol 84(9):4302–4310
- Vaidya NK, Ribeiro RM, Perelson AS, Kumar A (2016) Modeling the effects of morphine on simian immunodeficiency virus dynamics. PLoS Comput Biol 12(9)
- Van den Driessche P, Watmough J (2002) Reproduction numbers and sub-threshold endemic equilibria for compartmental models of disease transmission. Math Biosci 180(1–2):29–48
- Yuan CH, Di Mascio M, Perelson AS, Ho DD, Zhang L (2007) Determination of virus burst size in vivo using a single-cycle siv in rhesus macaques. Proc Natl Acad Sci 104(48):19079–19084
- Zhao X-Q, Borwein P (2003) Dynamical systems in population biology, vol 16. Springer
- Zhao X-Q (1995) Uniform persistence and periodic coexistence states in infinite-dimensional periodic semiflows with applications. Canad Appl Math Quart 3(4):473–495

Publisher's Note Springer Nature remains neutral with regard to jurisdictional claims in published maps and institutional affiliations.

Springer Nature or its licensor (e.g. a society or other partner) holds exclusive rights to this article under a publishing agreement with the author(s) or other rightsholder(s); author self-archiving of the accepted manuscript version of this article is solely governed by the terms of such publishing agreement and applicable law.

